Chapter 6
Feedback Control of Optically Trapped Particles

Jason J. Gorman, Arvind Balijepalli, and Thomas W. LeBrun

6.1 Introduction

Optical trapping is a family of approaches for localizing and manipulating atoms, molecules, and nano- and microscale particles using optical forces (see [1–4] for an introduction). Among these approaches, the gradient force optical trap, or *optical tweezers*, discovered by Ashkin et al. [5] is the most widely used due to its simplicity in implementation, applicability across both the micro- and nanoscales, and passive trapping stability. Ashkin's gradient force optical trap is the subject of this chapter and from herein will be referred to simply as an optical trap. In its simplest form, an optical trap is formed by directing collimated light from a laser into the back aperture of a microscope objective with high numerical aperture (NA), which is typically located on an inverted microscope. The microscope objective focuses the light to a diffraction-limited spot inside the sample of interest and then the light diverges after passing the focal plane, as shown in Fig. 6.1a. An optical trap is created near the focal spot and imparts optical forces on micro- and nanoscale particles within the vicinity of the trap. The shape of the beam results in the creation of two force components, a gradient force that pushes the particle towards the focus of the beam and a scattering component that directs the particle along the direction of propagation of the beam. A stable optical trap is formed when the gradient force is greater than the scattering force along all three Cartesian axes. Once in the trap, the particle will remain there until it escapes due to its own Brownian motion [6, 7] or is pushed out by an external force. Figure 6.1b shows multiple microscale particles held in optical traps.

The basic principles behind the generation of forces in an optical trap are well understood, although the development of accurate physical descriptions remains an

J.J. Gorman (✉) • A. Balijepalli • T.W. LeBrun
National Institute of Standards and Technology, 100 Bureau Drive,
Gaithersburg, MD 20899, USA
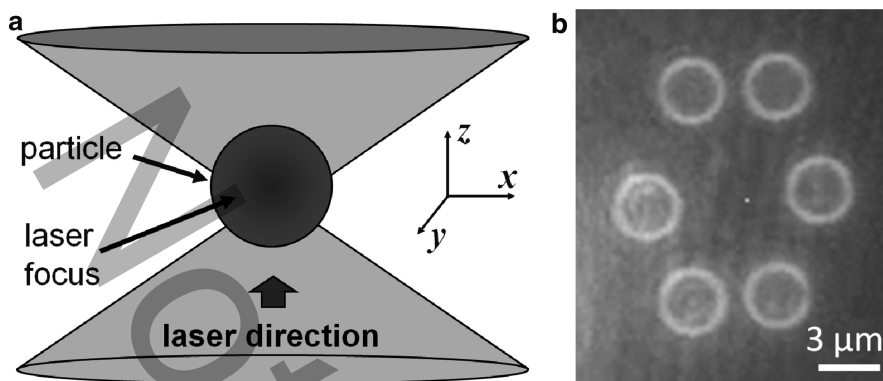e-mail: gorman@nist.gov; arvind@nist.gov; lebrun@nist.gov

Fig. 6.1 Optically trapped particles. (**a**) Schematic of an optical trap formed at the focus of a laser beam with a particle trapped at its center. (**b**) Simultaneous trapping of six microparticles using the time-sharing approach (optical microscope image). See [4] for a description of the time-sharing approach

open area of research (e.g., see [8–10]). For particles with critical dimensions larger than the wavelength of light used for trapping ($d \gg \lambda$, referred to as regime 1), these phenomena are generally described from the perspective of ray optics. The particle acts as a lens, thereby refracting the light and changing the direction of the momentum of the photons. Due to the conservation of momentum, the change in momentum of light causes an equal but opposite force on the particle. The sum of the forces from the rays of light pushes the particle towards the center of the trap as a result of the particle shape and the sharply focused laser. When the particle is smaller than the wavelength of light ($d \ll \lambda$, referred to as regime 2), a different perspective is used to explain the optical forces. The light's electric field imparts an oscillating electric dipole moment on the particle. This dipole moment is attracted to the point of highest intensity gradient, which is at the laser focus, resulting in the particle moving to the center of the trap. These two regimes provide a convenient way to think about the trapping physics but do not address the situation when the particle is approximately the same size as the wavelength of light. In reality, there is a continuum between these regimes but unified theories that describe the trapping phenomena across these regimes for all materials (e.g., generalize Lorenz–Mie theory [11, 12]) are complex and require extensive numerical calculations. Regardless of the regime, both descriptions above support the fact that in a stable trap, particles are drawn to the center of the trap and are held there until larger external forces push them out.

Particles ranging from tens of nanometers to tens of micrometers in diameter can be trapped (e.g., see [9]), although successful trapping across this range is heavily dependent on the shape and material of the particle. Spherical particles trap reliably due to their symmetry and ability to refract light across a wide entrance angle for the incoming light. As a result, spherical particles are most commonly used, although many other shapes have been trapped, as discussed shortly. The particle material

also has a large impact on the trapping forces, which can be easily explained using the two regime descriptions discussed above. In regime 1, the particle must be able to refract light and, therefore, is typically made of a dielectric material with the appropriate index of refraction, such as glass or polystyrene. Metals, which reflect and absorb light, do not trap well in this regime because they make poor lenses and they experience significant heating. Looking at regime 2, we find that the opposite is true. When particles are smaller than the wavelength of light they must be capable of generating a strong electric dipole moment. The strength of the dipole moment is directly related to the material's polarizability; the more polarizable the material, the larger the force. Since the polarizability of metals is significantly larger than for dielectrics, metal nanoparticles yield stronger trapping forces than their dielectric counterparts [13, 14]. In general, metal nanoparticles only trap when they are below several hundred nanometers in diameter, whereas dielectric particles trap from the microscale to the nanoscale, but not as effectively as metals at the nanoscale.

The effective restoring forces that push the particle toward the center of the trap can be conceptualized as a three-dimensional nonlinear spring. The magnitude of the forces is directly related to the intensity of the trapping light. The trapping forces can range from fractions of a piconewton to hundreds of piconewtons with the corresponding laser power ranging from a few milliwatts to hundreds of milliwatts. Photodamage of cells and macromolecules is one limiting factor in the laser intensity used [15, 16], and as a result limits the maximum forces that can be generated when manipulating biological components. Rohrbach [9] has shown that the trapping forces follow a nonlinear trend for dielectric particles as their diameter is reduced. Starting in regime 1, as the particle diameter decreases the trapping forces increase. When the wavelength of the trapping light and the particle diameter are equal, the trapping forces peak. As the diameter is reduced further, moving into regime 2, the trapping forces get smaller and approach zero for diminishing size. Similar behavior has also been demonstrated for gold nanoparticles, where the trapping forces decreased with decreasing particle diameter [17].

Once the particle is trapped it can be manipulated in all three Cartesian coordinates by moving the trap. Various actuators are used to move the trap within the sample to achieve a desired position or dynamic motion. In some cases, manipulation of multiple particles is necessary. A single laser can be used to create multiple traps to localize the position of multiple particles in different locations using a time-sharing approach. This is achieved by scanning the laser rapidly between several different locations where traps are to be formed [4]. By scanning the beam much faster than the response time of an individual particle, the intermittent trapping forces are still capable of maintaining the desired positions of the particles. An example of time-shared trapping is shown in Fig. 6.1b, where six microparticles are trapped simultaneously and rotated in a circle using one laser. Trap scanning can also be used to create traps of arbitrary shape by scanning the beam rapidly in a pattern to localize nonspherical particles. For example, line traps have been shown to be effective at trapping nanowires lengthwise in the image plane [18].

The applications of optical trapping are quite broad. In addition to simply manipulating a particle, a trapped particle can be used to impart forces on another

object or be used to measure small forces applied to the trapped particle by some other system of interest. A single trap or multiple traps can be used to pull or push objects, which can then be used for experimental mechanical measurements with exceptional precision due to the nanoscale positioning capabilities of an optical trap. More than any other research area, biophysics has adopted optical trapping as a primary research tool for measurement and manipulation and it has been instrumental in many important discoveries with respect to the mechanics of molecules and cells over the last two decades. Optical trapping has been used to investigate the nonlinear stiffness exhibited by DNA [19] and to measure the velocity of RNA polymerase steps during the transcription of DNA, as well as the pulling force of the RNA polymerase [20]. In these cases, one end of the DNA molecule was attached to a microsphere that was trapped and the other end was stuck to a glass slide either directly or through an additional molecule, such that the trapped microsphere could apply a tensile load to the DNA. Similar experimental approaches have been used to observe the folding and unfolding of single proteins [21] and to measure the pulling force and velocity of molecular motors, including myosin (critical in muscle contraction) [22] and kinesin (used in many cell functions) [23]. Optical trapping has also made a large impact on cell-level studies. For example, traps have been used to stretch red blood cells to measure their elasticity [24, 25], which is an excellent indicator of cell health, and to perform automated cell sorting for large assays that require high-quality cells [26].

Numerous measurement applications at the micro- and nanoscales beyond biophysics have also made use of optical trapping. Trapped particles have been used as local probes of fluid flow velocity [27] and viscosity [28] within microfluidic channels, providing *in situ* measurements that are otherwise difficult to achieve. The force characteristics of an optically trapped particle have also been used as a probe for measuring the topography of structures within an aqueous sample with minimal contact forces ($<5\,pN$). Similar to scanning probe microscopy, the trapped particle is scanned over a structure and the displacement of the particle is recorded to produce a representation of the structure topography [29–31]. Optical traps have also aided exploration into the fundamental physics of mesoscopic systems. For example, an optical trap was used to demonstrate that the instantaneous velocity of a Brownian particle can be measured [32], which was long believed to not be possible.

Another important application domain for optical trapping is the assembly of particles into more complex and functional micro- and nanostructures. Early work in this area focused on microstructures. For example, multiple optical traps were used to assemble linkages composed of cells and polystyrene microparticles that bond due to protein molecules that provide biospecific adhesion [33]. Linear chains of microparticles have also been assembled using a combination of optical trapping and photopolymerization to bond the particles together [34]. The resulting structures have been used to control particle flow in microfluidic channels and could be used as a probe for manipulating other microstructures. Trapping has also been used to automatically assemble a sixteen-piece microscale puzzle [35], which demonstrated that this approach is viable for low-throughput manufacturing. More recently, there has been a focus on assembling structures with nanoparticles. Nanowires have been

trapped and rotated in the plane and then assembled into free-floating linkages using laser-based cutting and bonding techniques [36]. It has also been shown that multi-nanowire structures can be assembled on a surface using an adhesive layer [37]. Recently, gold nanoparticles have been assembled into ordered patterns of forty or more using optical trapping with position deviations from the desired locations on the order of ± 100 nm [38]. Assembling nanoparticles and nanowires into nanodevices using optical trapping can be more time and cost efficient than many top–down and bottom–up fabrication approaches when prototyping devices. However, it is likely that it will not be appropriate for high-volume production due to its low throughput.

It is clear from the applications discussed above that users of optical trapping typically require a high level of control over both force and position, whether it be a measurement, manipulation, or assembly task. Furthermore, due to the optical forces, the interaction forces between the trapped object and the trapping medium, and the object inertia, the dynamics of a trapped particle are quite complex. As a result, the application of feedback control to optical trapping is an obvious approach to improving the system performance, whether it be for force or position control. This chapter focuses on the use of feedback control in optical trapping and is intended as an introduction to both the technical and practical issues. An overview of the existing research in this area is provided in the following section along with a discussion of the various control objectives encountered. This is followed by a discussion of the sensing and actuation technologies typically used in optical trapping and the tradeoffs in their performance with respect to closed-loop control. The dynamics of an optically trapped particle are then explored, with an emphasis on the control challenges and tractable models that can be used for control design. A control approach that uses the optical trap position as the control input (scan control) to suppress Brownian motion is then presented. Finally, the outstanding challenges in this field from our perspective are discussed.

6.2 Overview of Feedback Control in Optical Trapping

As with so many other fields, feedback control has been integrated with optical trapping in order to improve system performance and enable new capabilities. The earliest example of feedback control is the stabilization of levitated microparticles with optical forces, as demonstrated by Ashkin and Dziedzic [39]. However, in this case, the trapping forces for optical levitation are largely along the laser's direction of propagation rather than in all three Cartesian directions, as found in the gradient force optical trap. Feedback control was first applied to a three-dimensional gradient force optical trap by Finer et al. [22] to maintain a constant position for a trapped particle while a motor protein (myosin) pulls on the particle. The added stability of the particle provided by feedback control yielded force and position measurements that had the best sensitivity and resolution to date. Since then, single molecule biophysical experiments have been a driving force for control innovations in optical
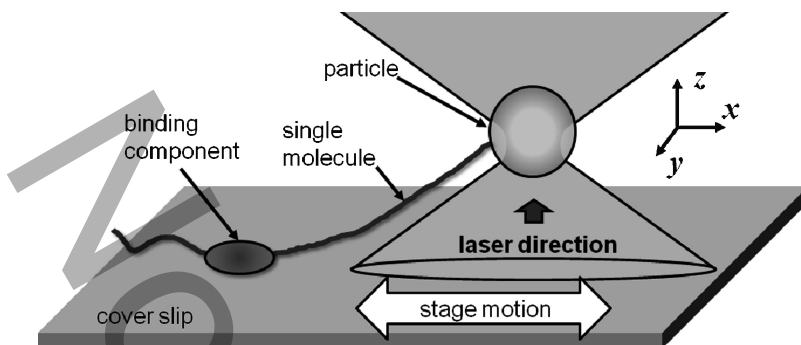
Fig. 6.2 Schematic of a common configuration for single molecule measurements using an optical trap. A single molecule is attached at one end to a trapped microparticle and attached to a binding component at another location along its length. Synchronized motion of the trap and coverslip is used to measure the mechanical properties of the single molecule, the binding component, or both

trapping and the use of feedback control has played a major role in a number of important studies [19, 20, 23, 40–44].

The majority of these single molecule studies can be viewed as variations on the trapping configuration depicted in Fig. 6.2. A microparticle is held in an optical trap close to the sample coverslip. A single molecule is attached to the microparticle at one of its ends and is attached to a binding component at another location along its length. The binding component is adhered to the coverslip through a selective chemical bond. In some cases, the binding component is a motor protein that can move along the single molecule or move on the slide, which in both cases will impart a force on the microparticle. Specific examples of this configuration include an actin molecule and myosin molecule [22]; a DNA molecule and RNA polymerase [19]; and a kinesin molecule and a microtubule [23], for the single molecule and binding component, respectively. The particle motion in an optical trap can be measured accurately using one of the methods described in more detail later in this chapter. For a properly calibrated optical trap, the trapping force can then be accurately measured as a function of the displacement of the particle, under the assumption that the trap acts like a nonlinear spring. Additionally, the coverslip, and therefore the binding component, can be moved relative to the trap using a precise motion stage. As a result, this configuration can be used to measure the motion and force characteristics of the single molecule or binding component through coordinated motion between the trap and stage. This coordination is where feedback control plays a critical role. Since the range of the particle in the trap where linear force measurements can be made is small (e.g., ~ 250 nm for a 1 μm particle), precise control over the position of the trap is needed to maintain the experiment in this range, which has been an enabling factor in the biophysical experiments discussed above.

Depending on the measurement of interest, the experimental configuration shown in Fig. 6.2 is typically implemented either isometrically (constant particle position) or isotonically (constant particle force). Isometric measurements are used to
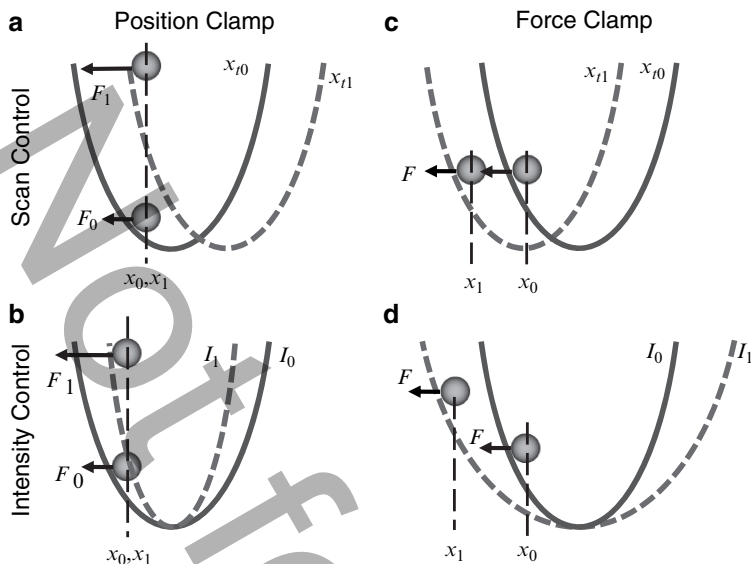
Fig. 6.3 A visual description of position and force clamps implemented with either scan control or intensity control. The optical trap is represented as a potential well and in each case is shown in two states, before (0) and after (1) control action. (**a**) Position clamp using scan control – the trap position is adjusted to keep the particle stationary. (**b**) Position clamp using intensity control – the laser intensity is adjusted to keep the particle stationary. (**c**) Force clamp using scan control – the trap position is adjusted to keep the force on the particle constant. (**d**) Force clamp using intensity control – the laser intensity is adjusted to keep the force on the particle constant. Adapted from Visscher and Block [43]

measure the mechanical properties of the single molecule or binding component (e.g., stiffness or pulling force of motor protein), whereas isotonic measurements are useful for tracking their motion over longer ranges (e.g., motor protein step size). In both cases, they are implemented using feedback control, either with a position clamp (isometric) [19,20,22,40–42] or a force clamp (isotonic) [23,43,44]. Feedback control for either clamping methods can be realized using one of the two control inputs to the system: the position of the trap or the intensity of trapping laser. As a result, there are four distinct control modes that are defined by whether position or force clamping is desired and whether the control input is the laser intensity or trap position, as depicted in Fig. 6.3.

The trap is drawn in Fig. 6.3 as a potential well and the trapped particle is shown in two states for each control scenario, before (state 0) and after (state 1) control action. A force, F, is applied to the particle through the single molecule, which pulls the particle away from the center of the trap. The trapping force that counteracts the external force F is proportional to the slope of the potential well at the position of the particle. When using a position clamp, the position, x, is held constant either by scanning the trap position, x_t, to the right (Fig. 6.3a) or by increasing the laser

intensity, I (Fig. 6.3b), to oppose the force. Alternatively, a force clamp can keep the reaction force constant either by scanning the trap to track the particle position (Fig. 6.3c) or by reducing the laser intensity as the particle is pulled away from the center of the trap (Fig. 6.3d). Note that the particle shown in Fig. 6.3d is at two different heights for the two states. In order to maintain a constant force on the particle, the location of the particle in the well shifts to maintain the same slope for the two states. Each of the control modes has its advantages depending on the biophysical experiment of interest, which are discussed in [43]. These modes provide the control architecture but the control law that determines the laser intensity or trap position at a given time instant must still be defined. In general, the position and force clamps demonstrated in [19, 20, 22, 23, 40–44] have been implemented using a proportional–integral–derivative (PID) control law, or some subset of this (e.g., P, PI), with static position or force setpoints.

Closed-loop position and force clamps have been the enabling factor in all of the biophysical measurements discussed above. However, as would be expected, the emphasis in this research has been on the biophysics and not on the optimization of the controller design. As a result, the controllers up to this point were implemented with minimal control design effort and without analysis of the tracking performance or suppression of the Brownian motion of the trapped particle. Furthermore, the bandwidth of these control systems was relatively low given the known dynamics of the particle. In most cases, the bandwidth is below 2 kHz due to the use of averaging filters. Finally, the results discussed above were almost exclusively focused on particles that are tethered to the coverslip by a molecule. The molecule localizes the particle and reduces its Brownian motion, thereby making it easier to control. Since there are many applications for optical trapping outside of biophysics that do not use a tether, there is a need for control systems for freely suspended particles that go beyond the force and position clamp control modes.

Within the past decade, control system researchers have begun to investigate general control design approaches for optically trapped particles based on the previous work on force and position clamps [45–52]. This research has been motivated by the large impact of the biophysical measurements described above and other broad applications for precise optical traps, including nanoscale assembly and material characterization. One major thrust has been the suppression of Brownian motion to improve the position localization of the particle. In general, this research has focused on the control of free particles rather than those that are tethered because the control approach can then be adapted for any specific application. Wulff et al. [45] investigated the performance of a proportional–integral (PI) controller that is tuned to achieve Bode's ideal first-order loop gain and found that it could suppress Brownian motion by 20% below 100 Hz for a 1 µm polystyrene particle, but it amplified the motion above this frequency. The limited bandwidth was partially due to the fast scanning mirror used to move the trap, which required an observer to estimate its scan angle and has slower dynamics than other commonly used scanners. An adaptive control approach was also demonstrated by this group, which can automatically identify the system parameters for different particle sizes,

particle materials, and laser power and then tune the controller appropriately [46]. High-bandwidth Brownian motion suppression was first demonstrated by Wallin et al. [47], where a linear proportional controller was used to increase the trap stiffness by a factor of 13 over a wide frequency range (DC to $\sim 5\,\mathrm{kHz}$). A proportional predictive controller was also investigated to extend the bandwidth of the controller by compensating for loop delays with an infinite impulse response (IIR) filter, resulting in an even greater trap stiffness and frequency range for motion suppression [48]. Most recently, we have presented an analysis of a general PID controller for Brownian motion suppression, including expressions for H_2 and H_∞ norms for the closed-loop system, and have experimentally demonstrated a reduction in the RMS motion of a $1\,\mu\mathrm{m}$ particle by approximately 40% compared to a static trap [49].

All of the controllers discussed above have been linear, although the stiffness of the trap is known to be nonlinear. The trapping force can be approximated by a linear stiffness near the center of the trap but the stiffness decreases as the particle moves away from the center and asymptotically approaches zero. From an energy perspective, the potential well formed by the trap has a finite depth and the particle can escape the potential well if its energy is large enough, which could either be due to the particle's thermal energy or an external force. As a result, there has been interest in developing nonlinear controllers that can guarantee that the particle remains in the trap, thereby enhancing manipulation capabilities. Such controllers have been developed [50–52] but have yet to be demonstrated experimentally. However, stability analysis and simulation results indicate that these nonlinear approaches can render the particle's motion globally asymptotically stable, such that the particle will remain trapped indefinitely barring any physical limitations of the experiment. These approaches warrant further study and need to be implemented in practice.

These advances in controller design have brought clear improvements in system performance, including enhanced disturbance rejection and wider operational bandwidth, compared to those used in previous force and position clamp research. However, control researchers have only begun to scratch the surface with optical trapping. The achievements discussed above only address particle localization or the zero setpoint regulation problem. Nonzero setpoint regulation, as found in position clamps, and tracking or following, as found in force clamps, have not been analyzed from the control perspective. Additionally, the majority of this work uses scan control instead of intensity control and as a result does not address the control of the particle position along the optical axis. One exception is our recent work on using intensity control to keep nanoparticles in the trap for much longer durations than found with a passive trap [53]. Finally, it is clear that there is still room for improvement in both the closed-loop bandwidth and resolution for optical traps. Increasing the bandwidth will enable added suppression of Brownian motion at higher frequencies, thereby improving the overall localization of the trapped particle. Increasing the resolution will improve the manipulation precision for particles during the assembly of heterogeneous structures, particularly at the nanoscale. Further, there are typically tradeoffs between bandwidth and

resolution that must be understood through analysis of the closed-loop system. One way of addressing some of these issues is through the selection of the best trap actuators and particle sensing methods for a given application.

6.3 Actuation and Sensing

The performance of the sensors and actuators within a servo control loop has a direct impact on the performance of the closed-loop system. Although in theory the controller can be designed to compensate for some shortcomings in actuator performance (e.g., dynamic inversion, pole/zero cancellation), in practice this often results in high control effort, which can have negative effects on the actuator. Therefore, it is important that the actuators and sensors are selected based on known performance goals. Optical trapping has many options when it comes to sensing and actuation with a wide range of tradeoffs. This section discusses some of the best options for feedback control and highlights the issues that affect closed-loop operation. A broader overview of these technologies with respect to optical trapping can be found in [3, 43].

As described previously, an optically trapped particle has two distinct control inputs: the laser intensity and the trap position. Therefore, there are two classes of actuators of interest: laser intensity modulators and trap scanners. As shown in Fig. 6.4, both actuators can be used simultaneously or separately depending on the application. Obviously, the particle position sensing system is important because it provides feedback for the controller but it is also used to perform measurements with the particle, such as indirectly measuring the external forces applied to the particle. These three components, laser trap scanner, intensity modulator, and position sensing system, are now examined.
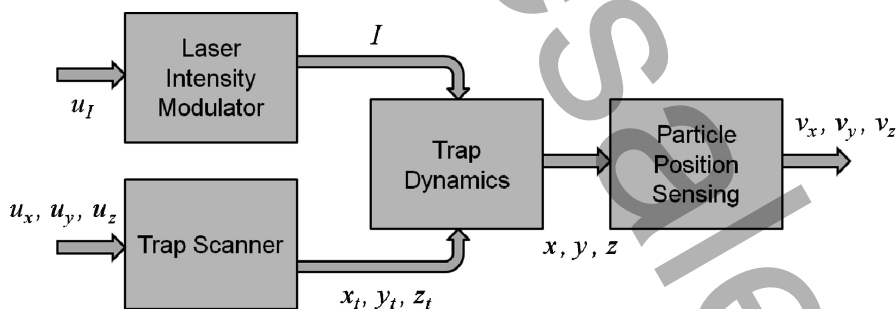

Fig. 6.4 Block diagram showing the relationships between the trap actuation, trap dynamics, and particle position sensing

6.3.1 Trap Scanners

In order to achieve trap scanning in the *x* and *y* directions (in-plane scanning), the laser beam must rotate about the back aperture of the microscope objective to avoid clipping the beam. This is achieved by locating the laser scanner, which alters the angle of the beam, at a plane conjugate to the back aperture (i.e., an object at the back aperture can be imaged at the plane of the scanner location) [54]. Rotating the beam about the back aperture also ensures that the beam does not get clipped at the aperture before entering the microscope objective. Spatial light modulators are widely used for laser scanning in optical trapping, particularly for holographic optical tweezers [55] and the generalized phase contrast method [56]. However, spatial light modulators have modest update rates that are not appropriate for closed-loop control and, therefore, are not covered further in this chapter. The most prevalent approach for scanning the beam for feedback control, thereby translating the trap, is with an acousto-optic deflector (AOD). AODs use acoustic waves to scan a laser at high rates. A radio frequency (RF) acoustic wave is generated inside a crystal using a piezoelectric transducer. This creates a periodic structure inside the crystal with areas of increased and decreased index of refraction that is analogous to a diffraction grating. This grating causes the incoming beam to be split into two beams, a diffracted and undiffracted beam, when the incoming beam is properly aligned to the Bragg angle, θ_{Bragg} (see Fig. 6.5a). Changing the frequency of the sound wave alters the period of the grating, resulting in an angular deflection of the diffracted beam (see [57, 58] for more details). The *xy* trap position can then be controlled through fine control of the input frequency. One major benefit of using AODs is that the scan bandwidth is typically on the order of 1 MHz, which is achieved with tunable RF frequency sources. Furthermore, AODs are widely available for different laser wavelengths and beam sizes. However, their main drawback is that they exhibit an inherent time delay caused by the time of flight of the sound wave between the transducer and the far side of the deflected beam. The time delay ranges from 1 µs to 30 µs depending on the size of the crystal and the beam diameter. Although this may seem small, within a closed-loop system this level of time delay will reduce the effective bandwidth of the system to tens of kilohertz and will set limits on the system stability. Most of the results reported to date have not been affected by this issue because their controller bandwidth was the limiting factor. However, recent results on Brownian motion suppression [47–49] have shown that the time delay sets a lower bound on the particle RMS motion that can be achieved with feedback. An additional drawback of AODs is that the sound wave causes wavefront distortion in the beam, causing nonideal behavior in the trap (e.g., the intensity profile may deviate from the expected Gaussian profile).

   Another important scanner option is the electro-optic deflector (EOD) [58], which has seen limited use in optical trapping [59] but is well suited for high-bandwidth control. An electro-optic crystal undergoes a change in its index of refraction when a high voltage (0 V to 1,000 V, depending on the material) is applied
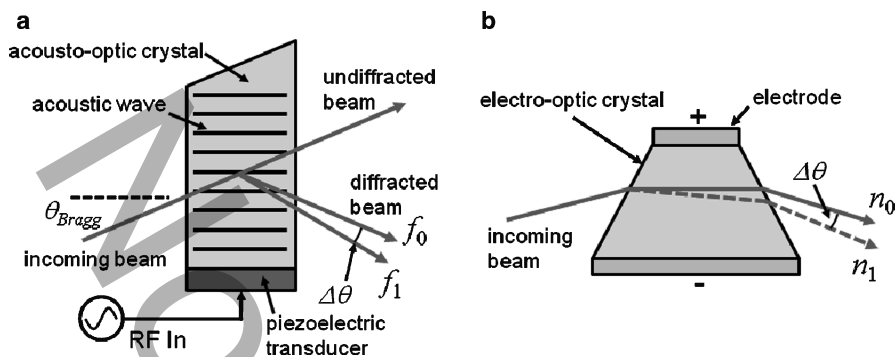
Fig. 6.5 Operating principles for acousto-optic and electro-optic deflectors. (**a**) Acousto-optic deflector (AOD). A laser beam enters the acousto-optic crystal at the Bragg angle, θ_{Bragg}. Half of the beam is unaffected and passes through. The other half is diffracted by the RF acoustic wave generated by the piezoelectric transducer. The exit angle of the diffracted beam is controlled by changing the acoustic wave frequency (exit beam shown at frequencies f_0 and f_1). (**b**) Electro-optic deflector (EOD). The index of refraction of an electro-optic prism is controlled by applying a voltage across the prism. As the index of refraction is changed, the beam's exit angle changes (shown at two different indices of refraction, n_0 and n_1)

across the crystal. As shown in Fig. 6.5b, when the crystal is shaped as a prism, the change in the index of refraction causes a change in the exit angle of the beam from the prism. In practice, the prism design is more complex than shown but the basic principal remains the same. Similar to the AOD, EODs have high scanning bandwidth but they do not suffer from a time delay like the AOD. As a result, EODs offer the fastest scanning response of any commercially available actuator. The bandwidth is only limited by the voltage amplifier rather than the electro-optic effect and scan rates on the order of hundreds of kilohertz are possible. The main disadvantages of EODs are that they have the smallest scan range among the most common scanner technologies and they can generate electromagnetic interference (EMI) due to the high drive voltage that can introduce noise into surrounding instrumentation.

Due to the high scanning bandwidth of AODs and EODs, they are the two best options for closed-loop operation of optical traps. However, scanning mirrors have also seen significant use in optical trapping and are, therefore, worth mentioning here. Scanning mirrors are electromechanical actuators that provide control over the tip and tilt of an attached mirror. The actuation mechanism for the rotational degrees of freedom can be achieved with a piezoelectric actuator, a voicecoil, or a galvanometer; each with its own advantages and disadvantages. The main benefits of using a scanning mirror for optical trapping are that they are easy to align and use, they reflect almost all of the beam power into the microscope objective, so very little power is wasted, and they have a negligible effect on the wavefront of the reflected beam. However, they almost universally have low scanning bandwidth

Table 6.1 Critical performance parameters for trap scanners (values based on commercially available systems)

Actuator type	Range (mrad)	Resolution (μrad)	Bandwidth (MHz)	Time delay (μs)
AOD	4–56	0.01–6	0.1–4	1–30
EOD	0.6–5	0.01–1	0.2–0.25	Negligible
Scanning mirror	1–350	0.02–1	0.0002–0.002	Negligible

due to the mechanical motion involved, with most systems scanning below 1 kHz. Additionally, they typically have more complex dynamics than AODs and EODs, including mechanical resonances, hysteresis, and nonminimum phase behavior. As a result, scanning mirrors are in general not well suited to fast feedback control for optical traps. However, they can be of use in low-bandwidth applications where their simplicity of use and minimal impact on beam quality are needed.

The most important performance parameters for trap scanners with respect to feedback control are scanning range, resolution, bandwidth, and the time delay if present. These parameters are summarized in Table 6.1 for AODs, EODs, and scanning mirrors based on commercially available systems known to have been used for optical trapping. Although AODs typically have the highest bandwidth of the three, the time delay in AODs limits their effective bandwidth within a feedback loop. As a result, EODs offer the best closed-loop performance if the small scan range is acceptable. Otherwise, AODs with short time delays are preferred for control. Compression mode, or longitudinal mode, AODs typically have the shortest time delays because the acoustic wave is propagated along a crystal axis that has a higher acoustic velocity, whereas shear mode AODs have longer time delays but larger scan ranges. Proper selection of the beam scanner can greatly simplify the control design for a given application.

Scanning the trap along the optical axis (z-axis) is much more difficult than in the x- and y-axes for feedback control. One approach is to use a piezoelectric scanner to translate either the sample or the microscope objective, thereby moving the optical trap relative to the sample. This approach typically results in low scanning bandwidth ($<200\,\mathrm{Hz}$) due to the mass of the objective or sample holder, which is generally inadequate for fast feedback control. Additionally, the complex dynamics of the scanner and its mechanical interactions with the coverslip on the sample make it a challenge to control. Surprisingly, few other options have been implemented. One intriguing possibility is to use AODs to control the height of the trap. Two AODs can be used in series to control the focus of a beam [60], which would in turn change the height of the trap, providing scanning bandwidth similar to that obtained with AODs for in-plane motion. Another possibility is to use a MEMS membrane mirror to control the beam focus [61], which could achieve a scanning bandwidth on the order of 5 kHz. The current lack of scanning options along the optical axis is a major limiting factor in obtaining precision three-dimensional control of particle position.
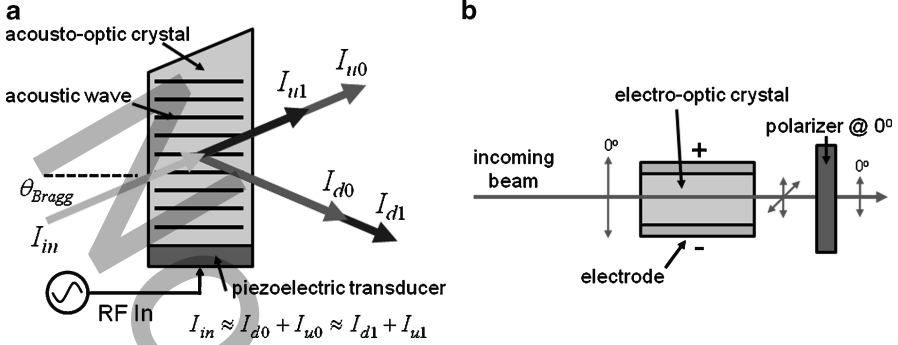
a

b

Fig. 6.6 Operating principles for acousto-optic and electro-optic modulators. (**a**) Acousto-optic modulator (AOM). The diffraction effect caused by the RF acoustic wave splits the incoming beam into two beams. The RF input power is used to tune the intensity ratio between these beams. (**b**) Electro-optic modulator (EOM). The incoming beam enters an electro-optic crystal that alters its polarization as a function of the control voltage. The beam then passes through a polarizer set at $0°$. The exiting intensity is reduced by shifting the laser polarization in the crystal away from $0°$

6.3.2 Laser Intensity Modulators

The stiffness of the trap is directly proportional to the laser power. Therefore, particle motion within a trap can be controlled by adjusting the laser intensity accordingly. The acousto-optic modulator (AOM) is the most common actuator used to control laser intensity and has been used previously in optical trapping to implement position clamps [19, 20]. An AOM operates similarly to an AOD in that an acoustic wave inside a crystal is used to create a diffraction grating that alters the incoming beam's direction (see Fig. 6.6a). However, instead of adjusting the frequency of the acoustic wave, its amplitude is controlled, which changes the amount of light diffracted by the wave. The sum of the optical intensities for both the diffracted and undiffracted beams remains relatively constant as the wave amplitude is changed. AOMs generally have time delays shorter than most AODs ($<5\,\mu s$). Therefore, the effective bandwidth in AOMs is typically higher in comparison to AODs, with most systems achieving at least 100 kHz. Similar to AODs, AOMs can cause wavefront distortion in the trapping beam due to the diffraction grating, which can result in undesirable deviations from the ideal beam profile.

An electro-optic modulator (EOM) can also be used to control laser intensity. An EOM is effectively a tunable waveplate, as shown in Fig. 6.6b. The beam entering the electro-optic crystal is linearly polarized at $0°$. The polarization of the beam exiting the crystal is controlled by the voltage applied across the crystal crosssection. After exiting the crystal, the beam passes through a linear polarizer set at $0°$. If the beam polarization is rotated away from $0°$ due to an applied voltage on the crystal, the intensity of the beam exiting the polarizer will be reduced accordingly. Similar to EODs, the bandwidth of EOMs is limited by the achievable slew rate for

Table 6.2 Critical performance parameters for laser intensity modulators (values based on commercially available systems)

Actuator type	Bandwidth (MHz)	Extinction ratio	Time delay (µs)
AOM	1–30	300:1–2,000:1	0.5–5
EOM	0.25–100	200:1–1,000:1	Negligible
Modulated laser diode	0.35–20	>1,000 : 1	Negligible

high-voltage amplifiers and is typically above 200 kHz. Unlike AOMs, EOMs have a negligible effect on the beam wavefront and can transmit up to 95% of the incoming intensity.

One other option for intensity control worth mentioning is intensity modulation of a diode laser. This requires the use of a diode laser for trapping, which has become prevalent over the last decade. It is common to achieve an intensity modulation bandwidth in the tens of megahertz using this approach, making it the fastest actuation mechanism discussed here. The main drawback is that the beam characteristics can change when going from high to low intensity, including the phase and wavelength. However, this may have only a marginal effect on controlling the trapped particle. The critical performance parameters for the three intensity modulators discussed here are shown in Table 6.2. All three approaches are capable of achieving bandwidth greater than 100 kHz, which has been found to be sufficient in previous research. Hence, one advantage of intensity control over scan control is that it is straightforward to achieve high actuation rates with any of the modulator options, which is not the case for scanners. Additionally, intensity control can be used to localize a particle along the z-axis, which is difficult with the available trap scanner options, although it cannot control the position of the particle arbitrarily.

6.3.3 Particle Position Sensing

A number of different methods have been developed to measure the position of an optically trapped particle with resolution approaching 1 nm, both for in-plane and out-of-plane motion. However, only a few of these methods are appropriate for closed-loop control. These methods are described here along with some of the shortcomings of other methods that are less suitable for feedback. By far, the most commonly used position sensing method has been back-focal-plane detection [4, 43, 62, 63], which can measure the in-plane or x and y motion of the trapped particle. As shown in Fig. 6.7a, the back-focal-plane detection method uses a second laser to measure displacement by focusing the beam with the trapping objective and measuring the motion of the light scattered by the trapped particle. The advantage of using an independent laser for position measurement is that it provides a fixed reference, which yields absolute position measurements. The detection laser intensity is much lower than the trapping laser to minimize the trapping forces generated by this second beam. An idealized depiction of the relationship between the particle displacement and the motion of the light for dielectric particles is shown
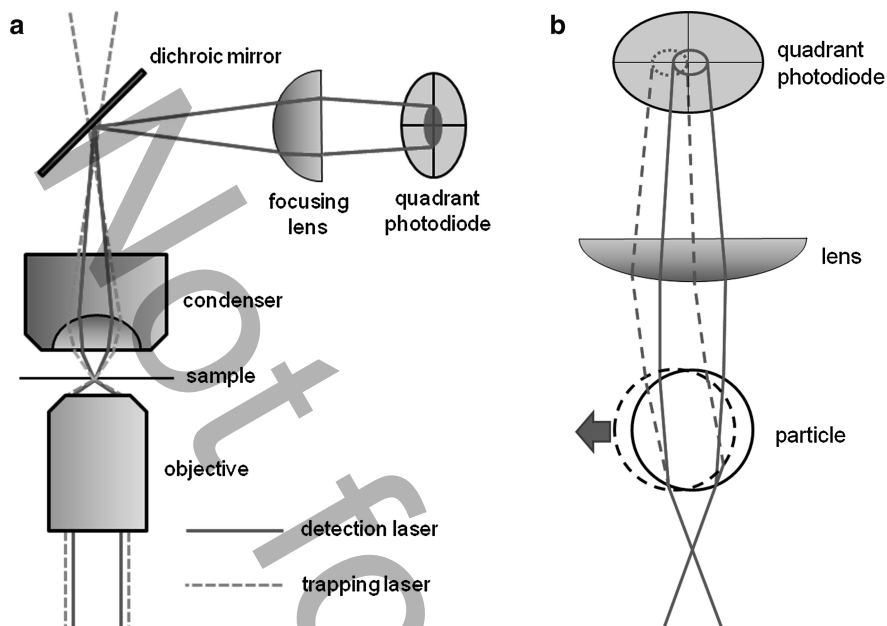
Fig. 6.7 Description of the back-focal-plane detection method. (**a**) Both the trapping laser and detection laser pass through the sample and are then separated with a dichroic mirror. The detection laser is directed onto a quadrant photodiode positioned near a conjugate plane of the back-focal-plane of the condenser. (**b**) Lateral motion of the particle results in scanning of the detection laser, which can be measured on the quadrant photodiode

in Fig. 6.7b. The detection laser is focused just below the trapped particle such that the particle collimates the light passing through it. In-plane motion of the particle results in angular scanning of the beam. The detection laser exiting the microscope condenser is then directed onto a quadrant photodiode by a dichroic mirror. The detection laser is generally a different wavelength than the trapping laser so that the two can be separated optically. The quadrant photodiode measures the motion of the beam, which can then be related to the particle motion through calibration (e.g., see [44]). This approach is referred to as back-focal-plane detection because the quadrant photodiode is placed at a plane conjugate to the back-focal-plane of the condenser. However, this exact placement is not required and the position of the quadrant photodiode along the optical axis is usually optimized empirically to maximize the displacement signal. Achieving a resolution and bandwidth of 1 nm and 100 kHz, respectively, is typical.

Several improvements on this method have been developed that could be beneficial for closed-loop control. One is the use of a differential back-focal-plane measurement in which two detection beams are used, one to track the particle of interest and the other to measure the motion of the microscope [64]. This approach has been used to counteract instrumentation drift and has yielded displacement resolution below 0.4 nm due to the cancellation of common mode disturbances.

Another approach has been developed to improve the sensing bandwidth, where the forward-scattered beam is segmented into two halves and each half is directed onto a separate fast photodiode rather than a quadrant photodiode [32]. Taking the difference between the two photodiode signals provides the same information for a single axis as for the quadrant photodiode but with a higher bandwidth, which was 75 MHz in this case. Control experiments have yet to require bandwidths in this range but it may be needed as experiments progress towards air or vacuum trapping environments where there is significantly less damping from the trapping medium surrounding the particle.

There are also variations on back-focal-plane detection pre-dating the use of two separate lasers, one for trapping and one for sensing, that are less appropriate for feedback control. Microscope illumination can be used to measure particle motion by imaging the particle onto a quadrant photodiode [22, 40, 41]. However, the light intensity is significantly lower than that from a laser and, therefore, the shot noise is much higher for a given bandwidth. The increased noise results in worse position resolution and as a result this method is not the best option for control. Another option is to use the trapping laser for both trapping and measuring the position of the particle by directing the forward-scattered light of the trapping laser onto a quadrant photodiode [4, 62]. This provides a measure of the particle's position with respect to the center of the trap, which can be useful for some experiments. However, as pointed out in [43], decoupling the position sensing from the trap scanning is necessary to provide particle position with respect to an inertial reference frame for feedback control. As a result, this method is typically not used for control.

Other methods for in-plane particle position measurement include laser interferometry based on differential interference contrast [65, 66] and image processing using digitized video of the particle [67, 68]. The former method can yield excellent resolution (~ 0.3 nm resolution over 100 kHz in [65]) but can only measure motion in one in-plane direction making it impractical for most applications. The latter method currently suffers from strict bandwidth limitations. Compensation for instrument drift using feedback from image processing has been demonstrated with a video sampling rate of 25 Hz [69]. However, this bandwidth is not suitable for the suppression of Brownian motion or fast trajectory following. Due to recent innovations in the design of high-speed digital cameras, images of trapped particles can be captured in excess of 2.5 kHz [70] but real-time image processing of the particle position remains a challenge. A conservative estimate for the current limit on the sampling rate of an image processing-based controller is 500 Hz but this will likely increase as parallel computation and field programmable gate arrays (FPGAs) are applied to this problem.

Particle sensing along the optical axis (z-axis) has rarely been used for feedback in a gradient force optical trap. However, there is clearly a need to move from the two-dimensional control described in [19, 20, 22, 23, 40–44] to complete three-dimensional control for nanoassembly and lower noise biophysical experiments. Two laser-based methods have been demonstrated for optical trapping that can be used for this purpose. The first method assumes that the detection laser passes through the particle and the refraction of the exiting light is modulated by the axial motion of the particle [29, 71, 72]. As shown in Fig. 6.8, the particle motion causes
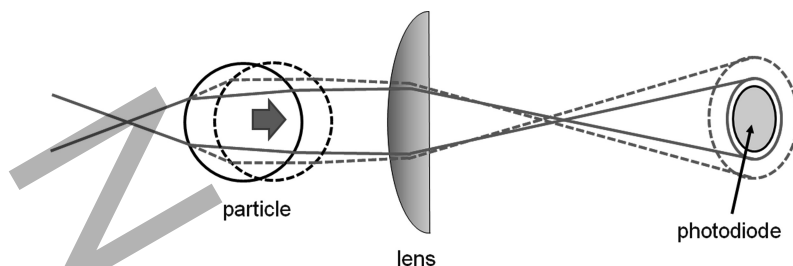
Fig. 6.8 Schematic of the optical detection mechanism for motion along the optical axis. The particle sits just upstream from the focus of the trapping and detection lasers. Light passing through the particle is refracted by the particle and is then passed through a lens (condenser and focusing optics). The exiting beam is focused to a point and then diverges. The diverging beam is positioned on a photodiode such that half of the intensity is on the photodiode for the nominal position. As the particle moves along the optical axis, the angle of refraction for the light passing through particle changes, thereby changing the intensity on the photodiode

more or less intensity to hit a photodiode located near a conjugate plane of the back-focal-plane of the condenser. The best position sensitivity is typically achieved when the photodiode is overfilled such that only half of the laser intensity is detected by the photodiode. The second method assumes that some of the detection laser is refracted by the particle while the rest is reflected, which is typically true for particles smaller than the wavelength of the detection laser [73, 74]. Interference between the refracted and reflected light results in a position-dependent intensity at the back-focal-plane of the condenser, which can be measured with a photodiode. Although these two methods leverage different physical phenomena it is difficult to separate them, particularly for particles below 1 μm. As with the back-focal-plane detection method described above, an independent detection laser is recommended for both of these methods to decouple the sensing and actuation. In-plane and out-of-plane sensing have also been combined for xyz measurement of the particle [72–74].

One of the major benefits of the laser-based position sensing methods described above is that the sensing bandwidth is only limited by the photodiode response and the dynamics of the readout electronics. In general, 1 MHz can be achieved with modest effort, which is more than suitable for the control applications proposed to date. However, sensor noise sets the ultimate limit on resolution and as a result, there is generally a direct trade-off between sensor resolution and bandwidth since wider bandwidth introduces more noise. Designing the positioning sensing system to have only the required bandwidth will maximize resolution and reduce the constraints on the controller design. The main sources of noise in these laser-based methods are intensity fluctuations and pointing instabilities in the detection laser, shot noise and Johnson noise in the photodiode and respective electronics, and mechanical vibrations due to acoustic or base excitations. Readers interested in an overview of noise considerations should refer to Gittes and Schmidt [75].

6.4 Dynamic Behavior of Optically Trapped Particles

The dynamics of an optically trapped particle are unique in that the optical forces have a limited operational range around the center of the trap. In this section, the finite trapping lifetime of particles is discussed to highlight some of the challenges in controlling trapped particles. This is followed by the development of an empirical dynamic model of a trapped particle that is suitable for control design.

6.4.1 Finite Lifetime in an Optical Trap

One of the most distinctive characteristics of the dynamics of an optically trapped particle is that the particle has a finite lifetime within the trap, meaning that the particle can escape from the potential well. This can be seen experimentally when trapping particles with low laser intensity, where the low trapping forces can only keep the particle in the trap for a short time. This phenomenon can be explained by noting that the potential well formed by the trap has finite depth since there is a limit on the trap width and depth set by the optics and laser power. If the particle reaches the edge of the well due to Brownian motion it can escape the trap or go back down into the well. Since Brownian motion is stochastic it is necessary to discuss the escape time, or lifetime, in a probabilistic sense, typically as a mean value. In this section, two methods for investigating trapping lifetime are discussed to highlight the challenges in controlling trapped particles.

An optically trapped particle can be considered as a mass–spring–damper system with a softening nonlinear spring. Assuming that the trapped particle is an ideal sphere, the inertial and damping components in the dynamics are relatively straightforward and are a function of the particle size and the material properties of the particle and trapping medium. However, the trapping forces are more difficult to model. Both experimental (e.g., see [41]) and theoretical results (e.g., see [76]) have shown that the qualitative behavior of the conservative optical trapping forces can be approximated with reasonable accuracy using a Gaussian potential well model. In reality, the optical forces along each axis are coupled to the motion along all three axes. However, for the purpose of discussing trapping lifetime, a one-dimensional Gaussian potential is considered here. The potential energy of the particle, V, can be written as $V = -\alpha e^{-\mu x^2}$, where x is the particle position with respect to the center of the trap. Ignoring the parameters α and μ for the time being, one can see that the potential energy resulting from optical forces approaches a constant value as x gets larger, as shown in Fig. 6.9a. The trapping force resulting from this model is found by taking the negative derivative of V with respect to x such that $F_t = -\partial V / \partial x = -2\mu \alpha x e^{-\mu x^2}$. As shown in Fig. 6.9b, the optical force is zero at the trap center, it increases while moving away from the center until it peaks, and then decreases until it reaches zero again. Intuitively, when the particle moves past the point of peak force the force pulling the particle back to the center is decreasing
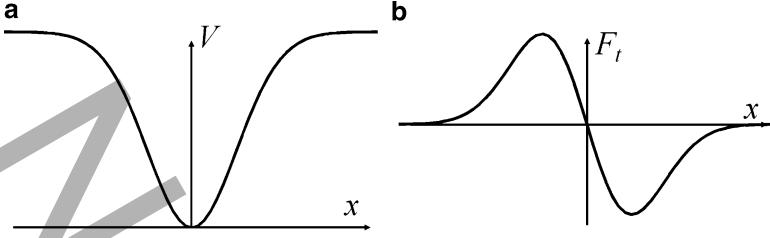
Fig. 6.9 The potential energy and force curve for the optical forces on a trapped particle. (**a**) The potential energy of a particle along one axis. (**b**) The resulting optical force as a function of displacement from the trap center

and, therefore, the particle can escape if Brownian motion drives the particle further away from the trap.

The Fokker–Planck equation [77] can be used to estimate the lifetime of a trapped particle. The time evolution of the probability density function (PDF), $W(x, t)$, for a particle under the influence of an optical trapping force is given by the Fokker–Planck equation shown in (6.1), which can be solved numerically. In this case, the optical trapping force, $F(x)$, is modeled using a Gaussian potential. The other parameters in (6.1) are the diffusion constant, $D = k_B T / \gamma$, Boltzmann's constant, k_B, the temperature of the fluid, T, and Stokes' constant, $\gamma = 6 \pi \eta a$, where a is the particle radius and η is the fluid viscosity.

$$\frac{\partial}{\partial t} W(x, t) = -\frac{\partial}{\partial x} D \left(\frac{1}{k_B T} [W(x, t) F(x)] - \frac{\partial}{\partial x} W(x, t) \right). \qquad (6.1)$$

The initial conditions for (6.1) are defined by a normalized PDF, $\varphi(x)$, (6.2), which describes the initial distribution of the particles in the trap. The function $\varphi(x)$ is selected so that the particle ensemble has filled the well at $t = 0$. The boundaries of the trap are defined over the closed interval $[-x_R, x_R]$. This absorbing boundary condition is shown in (6.3).

$$W(x, 0) = \varphi(x), \qquad (6.2)$$

$$W(-x_R, t) = W(x_R, t) = 0. \qquad (6.3)$$

The Fokker–Planck equation has been solved numerically using Mathematica. The solver first converts the partial differential equation (PDE) into a system of ordinary differential equations (ODEs) using a technique called the method of lines. It then solves this system of ODEs using either an implicit backward difference formula numerical integration technique or the Adams multi-step method, depending on the stiffness of the equations. The numerical solution of the PDE yields the PDF, $W(x, t)$, which can then be integrated over the density in the well to extract trapping
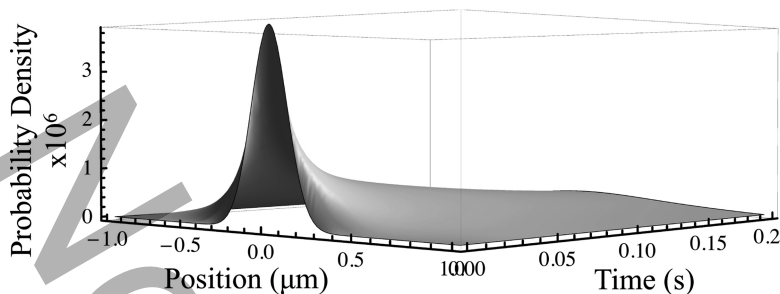
Fig. 6.10 A plot of the probability density function (PDF) as a function of time for a 100 nm gold nanoparticle in a weak optical trap. The flattening of the PDF as time progresses shows that the particle is likely to leave the trap within the time of this simulation

lifetime. This approach can also be used to determine the stability of a controller by augmenting the analyzed dynamic system with the controller and then solving the equations for an array of control parameters.

A representative PDF for a 100 nm gold nanoparticle in a weak optical trap is shown in Fig. 6.10. The power of the trapping beam is 1.5 mW and the corresponding depth of the trapping potential is calculated to be $1.14 k_{\mathrm{B}}T$. It can be seen in the figure that initially, the particles are located close to the center of the well, as indicated by the large peak at the center at $t = 0$ s. However, as the particles diffuse, they quickly escape the trap and the central peak, which is proportional to the number of particles inside the trap, decays exponentially. All of the relevant information pertaining to the behavior of the particle in the trap, such as the trap lifetime and average power absorbed by the particle, can be obtained by operating on this PDF. Trapping lifetime is directly related to the strength of the trapping laser intensity and the size of the particle. A microscale particle trapped with tens of milliwatts of power can in theory stay in the trap for weeks or months on average whereas a nanoparticle trapped with a few milliwatts of power may only stay in the trap for a few seconds.

A more physically accurate approach for simulating the stochastic nature of optically trapped particles is to combine a trapping force model obtained using generalized Lorentz–Mie theory (GLMT) [11,78] with Brownian dynamics simulations [79]. GLMT, which is applicable to a wide range of particle sizes and materials, has been used to calculate the optical force on the particle as a function of position in the x, y, and z directions for a 350 nm particle trapped with a laser beam with a wavelength, $\lambda = 1064$ nm. The force field is calculated over a closed interval of $\pm 3 \, \mu$m along the x- and y-axes and $(-2, +6) \, \mu$m along the z-axis, with a uniform grid spacing along all axes of 75 nm. Figure 6.11 shows 100 simulated trajectories of 350 nm glass nanoparticles under the influence of a GLMT-calculated force field with a beam power of 5 mW. The total trapping force along the z-axis generated by the GLMT model is overlaid on top of the nanoparticle trajectories in Fig. 6.11. The thick black line in the figure represents the total axial trapping force, including
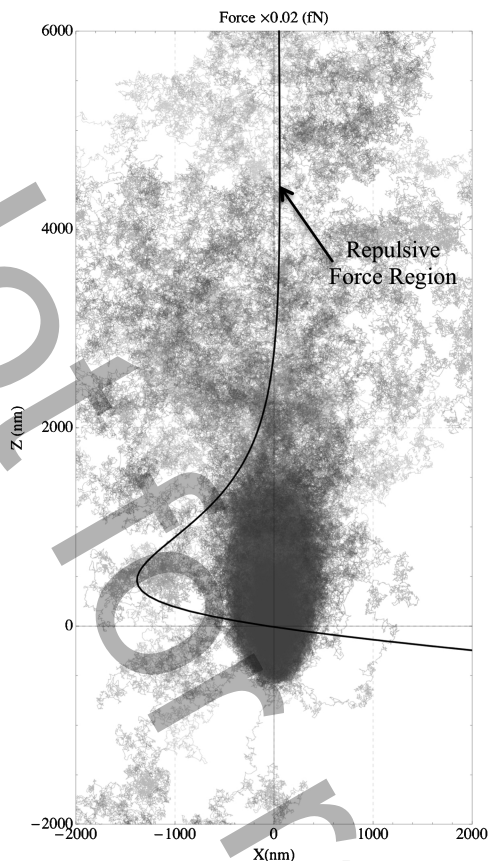
Fig. 6.11 Simulated motion of nanoparticles in an optical trap in the *xz* plane. 100 trajectories are shown with most of them exiting along the *z*-axis. The densely populated region around (0, 0) represents the stable part of the trap. The black curve is the force profile of the trap along the optical axis. Note that the force becomes repulsive approximately $3\,\mu m$ above the center of the trap

gradient and scattering components (directed along the positive *z*-axis). From the figure, it can be seen that the trapping force is attractive on either side of $z = 0$ and the magnitude of the attractive force is much larger on the negative side of the origin. On the other hand, when $z > 0$, the trapping force reaches a maximum at approximately $500\,nm$ and then decreases, eventually becoming repulsive at approximately $3.0\,\mu m$. The combination of weak gradient forces and axially directed scattering forces results in particles escaping preferentially along the positive *z*-axis as seen from the figure. The preferential exit along the optical axis is not surprising since the axial stiffness is always found to be lower than the lateral stiffness and the disruptive scattering component of the trapping force has a strong longitudinal component. These simulations show that a vast majority of particles exit along the optical axis, confirming that this is the primary issue in particle trapping lifetime

for a single beam optical trap. This behavior has also been observed qualitatively in trapping experiments in our laboratory.

These two numerical examples provide insight into the behavior of optically trapped particles that can influence controller design. Maybe even more important, both the Fokker–Planck equation and Brownian dynamics simulations have the ability to be used as control design tools through iterative solution for different control parameters and functions, providing a method for controller optimization. These numerical approaches have largely not been explored but may provide a viable solution for stochastic control systems in which the dynamic behavior is beyond the capabilities of standard optimal control methods.

6.4.2 An Empirical Model for Control Design

In this section, an empirical closed-form dynamic model for an optically trapped particle is derived for the purposes of control design. This model represents the in-plane dynamics (x and y directions) and does not describe motion along the optical axis (z direction). Following this derivation, the model is linearized for the control design discussed in the next section.

The equations of motion are derived using the energy method. The position of the particle in the plane is represented by the generalized coordinates x and y, and the inputs to the system for scan control are the trap coordinates, x_t and y_t, where all variables are defined with respect to the sensing coordinate system, which is an inertial reference frame (see Fig. 6.12). The kinetic energy, T, and potential energy, V, for the particle, and the generalized forces applied to the particle, Q_x and Q_y, can be written as:

$$T = \frac{1}{2} m \left(\dot{x}^2 + \dot{y}^2 \right), \tag{6.4}$$

$$V = \frac{1}{2} \alpha \left(1 - e^{-\mu r_t^2} \right), \tag{6.5}$$

$$Q_x = -\beta \dot{x} + \gamma \Gamma_x(t), \tag{6.6}$$

$$Q_y = -\beta \dot{y} + \gamma \Gamma_y(t), \tag{6.7}$$

where m is the mass of the particle, the parameter α is proportional to the laser power, and μ is a function of the beam waist of the trap and the radius of the trapped particle. The potential energy of the trapped particle is described by a two-dimensional Gaussian potential, where r_t is the distance between the center of the particle and the center of the trap (see Fig. 6.12), and can be written as:

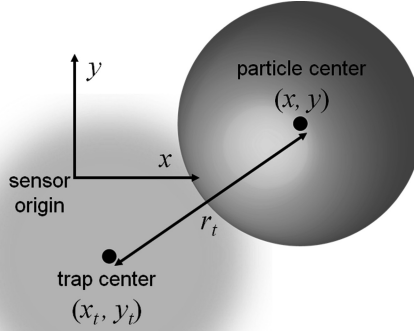$$r_t = \left((x - x_t)^2 + (y - y_t)^2 \right)^{1/2}. \tag{6.8}$$

Fig. 6.12 The trapping coordinate system

In (6.6) and (6.7), β is the damping coefficient, which for a spherical particle is defined by Stokes' Law as $\beta = 6\pi\eta r_p$. The parameter η is the viscosity of the trapping medium, which is a function of the absolute temperature of the trapping medium, T, and r_p is the radius of the particle. The second term in both (6.6) and (6.7) is the Langevin force, which is a stochastic force that results in Brownian motion. The parameter $\gamma = (2\beta k_B T)^{1/2}$, and $\Gamma_x(t)$ and $\Gamma_y(t)$ are Gaussian white noise processes [6, 7], and the parameter k_B is the Boltzmann constant.

Applying Lagrange's equations [80] using (6.4)–(6.8) results in the following equations of motion:

$$m\ddot{x} + \beta\dot{x} + \alpha\mu(x - x_t)e^{-\mu r_t^2} = \gamma\,\Gamma_x(t), \tag{6.9}$$

$$m\ddot{y} + \beta\dot{y} + \alpha\mu(y - y_t)e^{-\mu r_t^2} = \gamma\,\Gamma_y(t). \tag{6.10}$$

It can be seen in (6.9) and (6.10) that the motion along the x- and y-axes is coupled through the nonlinear stiffness of the trap. This nonlinear model can be simplified by: (1) noting that the inertial components are small compared to the damping and stiffness terms, and (2) the trapping force can be linearized about the center of the trap for small displacements. Therefore, the order of the system can be reduced by setting $m = 0$ and linearized about the origin using a Taylor series approximation, yielding the final reduced-order linearized equation of motion.

$$\dot{x} = -\frac{\alpha\mu}{\beta}(x - x_t) + \frac{\gamma}{\beta}\Gamma_x(t). \tag{6.11}$$

The equation of motion for the y-axis is the same as (6.11) except for the substitution of y for x and y_t for x_t. This linearized dynamic model is valid within a range about

the center of the trap that is dependent on the beam spot size and particle diameter (e.g., ± 250 nm for a $1\,\mu$m particle). This model has been assumed in the majority of previous work on controlled optical trapping (e.g., see [41,45–48]) and will be used throughout the rest of the chapter.

The product $\alpha\mu$ in (6.9)–(6.11) is the linear trap stiffness such that $k = \alpha\mu$. When implementing scan control, the control inputs are the trap position coordinates x_t and y_t. Therefore, the control inputs are not affine in the nonlinear dynamics, (6.9) and (6.10), but are affine in the linearized model. When implementing intensity control, the laser intensity control input is introduced through the parameter α, such that $\alpha = \alpha_0 I(t)$, where $I(t)$ is the laser intensity. One can see that the laser intensity directly affects the trap stiffness since $k = \mu\alpha_0 I(t)$.

Before closing this section, simple models of the sensor and actuator for scanning control are described. In the following section, scan control using an acousto-optic deflector (AOD) is presented. The AOD and drive electronics have first-order dynamics and a time-delay, but these dynamics do not affect the closed-loop system in the frequency range of interest in this discussion. Therefore, they are modeled as a linear gain, and can be written in the Laplace domain as:

$$x_t(s) = k_{\text{AOD}_x} u_x(s), \tag{6.12}$$

where k_{AOD_x} is the gain. The output signal from the quadrant photodiode used in back-focal-plane detection has been shown to be nonlinear [44, 62], and it approximately matches the derivative of a Gaussian potential. Therefore, the sensor function can be written as:

$$v_x = k_x x e^{-\varepsilon_x x^2}, \tag{6.13}$$

where k_x is the sensitivity of the sensor, and ε_x determines the zero-slope point for the error function. Calibration data for back-focal-plane detection is shown in Fig. 6.13 along with a least-square fit, showing a close fit between the data and model. In the control design discussed in the next section, the sensor response is linearized for the purpose of control design, such that $v_x = k_x x$.

6.5 Brownian Motion Suppression Using Feedback Control

In this section, an experimental instrument for optical trapping is described and a method for selecting the gains for a PID controller is presented for optimal suppression of the Brownian motion of the particle in the trap. Experimental results for this control system are then discussed.
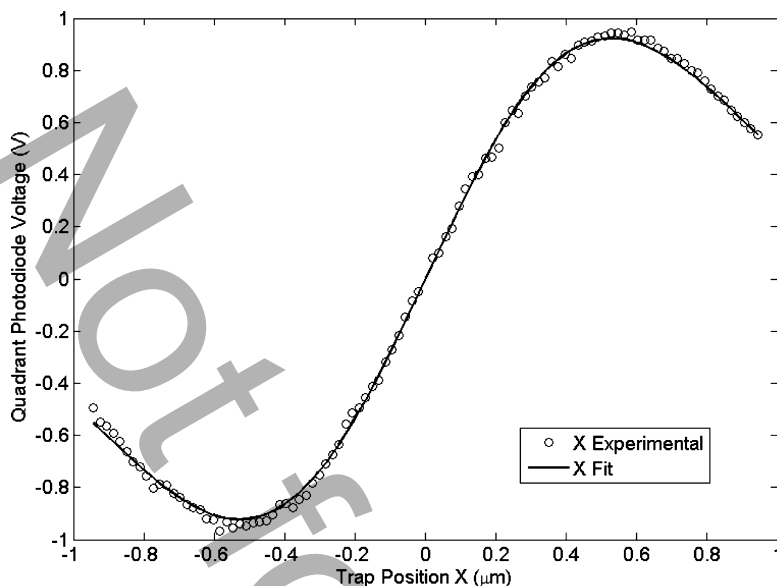
Fig. 6.13 Quadrant photodiode output voltage as a function of particle displacement for back-focal-plane detection (experimental data and fit curves for (6.13))

6.5.1 Instrument Design

A diagram of the optical layout of the optical trapping instrument is shown in Fig. 6.14. The optical layout utilizes two lasers: a Nd : YVO$_4$ laser with a 1064 nm wavelength for trapping and a diode laser with a 640 nm wavelength for detecting the trapped particle's position. The collimated trapping laser passes through an XY acousto-optic deflector (AOD), where it is scanned along two axes. A telescope then expands the beam to overfill the back aperture of the microscope objective. The telescope also ensures that the exit aperture of the AOD is at a plane conjugate to the back aperture of the microscope, so that the beam rotates about the back aperture rather than translate. The trapping beam is combined with the detection beam through a dichroic mirror. Both beams are directed into the microscope objective using another dichroic mirror and the beams then pass through the sample. The power of the detection laser at the focal plane is less than 1 mW, whereas the trapping laser power is typically between 30 mW and 150 mW. Therefore, the detection laser only has a negligible effect on the trapping dynamics. The microscope objective and dichroic mirror are mounted on a commercial inverted microscope.

Back-focal-plane detection is used to measure the position of the trapped particle, as described in Sect. 6.3.3. After exiting the sample, the detection beam is reflected by a dichroic mirror and passed through a lens, which focuses the beam onto a quadrant photodiode, where the deflection of the beam due to particle motion is measured. The quadrant photodiode in the back-focal-plane detection system has a
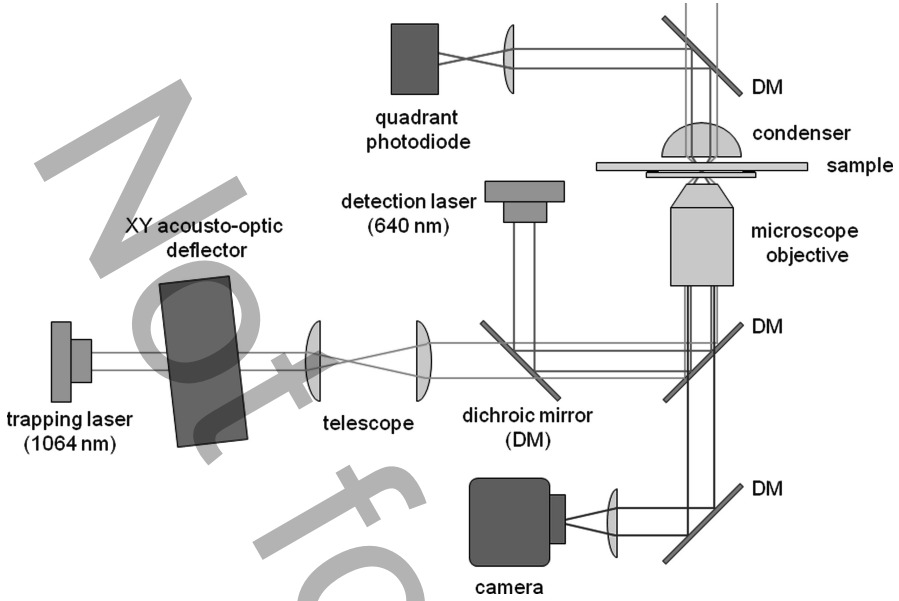
Fig. 6.14 A simplified diagram of the optical trapping instrument

bandwidth of 100 kHz. The sample is composed of a glass slide with a coverslip attached using double-sided tape. The chamber formed by this coupling is filled with a dilute solution of 1 μm diameter silica spheres in deionized water.
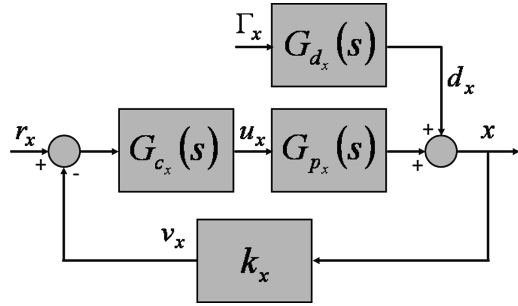
The position of the optical trap is controlled by the AOD. As is typical of acousto-optic crystals, the AOD introduces a time delay due to the time of travel of the acoustic wave in the crystal (approximately 27 μs in this case). Its scanning bandwidth is 30 kHz. As a result, the AOD is the limiting component in terms of loop rate. Although not considered within the following analysis, this limitation will be discussed with respect to the experimental results.

6.5.2 Design of a Scan Controller

As described previously, there are many different control objectives that can be pursued with optical trapping, including position tracking, force control, and particle localization. In this section, a linear controller design is presented for the suppression of Brownian motion. In (6.9) and (6.10), the Gaussian white noise processes $\Gamma_x(t)$ and $\Gamma_y(t)$ act as disturbances to the particle motion, resulting in Brownian motion. A PID controller that provides disturbance rejection of the white noise is presented here. The reduced-order linearized system is utilized in order to simplify the closed-loop analysis. Equation (6.11) can be written in the Laplace domain as:

$$x(s) = \frac{a}{s+a}x_t(s) + \frac{b}{s+a}\Gamma_x(s), \tag{6.14}$$

Fig. 6.15 Block diagram of the linearized closed-loop system

where $a = k/\beta$ and $b = \gamma/\beta$. Substituting (6.12) into (6.14) results in the following equation:

$$x(s) = G_{p_x}(s)u_x(s) + G_{d_x}(s)\Gamma_x(s), \tag{6.15}$$

where

$$G_{p_x}(s) = \frac{a k_{\mathrm{AOD}_x}}{s+a}, \tag{6.16}$$

$$G_{d_x}(s) = \frac{b}{s+a}. \tag{6.17}$$

The linearized closed-loop system can be drawn as shown in Fig. 6.15, where $G_{c_x}(s)$ is the controller transfer function, $r_x(s)$ is the command input, and the input to the controller is the control error $e_x(s)$, which can written as:

$$e_x(s) = r_x(s) - v_x(s). \tag{6.18}$$

However, in this case we are not interested in the tracking problem and only look at the disturbance rejection properties of the controller. Therefore, r_x is set equal to zero and the closed-loop transfer function can then be written as:

$$x(s) = G_{\Gamma_x x}(s)\Gamma_x(s), \tag{6.19}$$

where

$$G_{\Gamma_x x}(s) = \frac{G_{d_x}(s)}{1 + k_x G_{p_x}(s)G_{c_x}(s)}. \tag{6.20}$$

The standard PID form [81] is used for the controller,

$$G_{c_x}(s) = \frac{K_{\mathrm{d}}s^2 + K_{\mathrm{p}}s + K_i}{s}, \tag{6.21}$$

where K_{p} is the proportional gain, K_{i} is the integral gain, and K_{d} is the derivative gain.

Equation (6.19) defines the closed-loop response of the particle motion to the thermal noise that causes Brownian motion. Given (6.21) as the controller, the transfer function $G_{\Gamma_x x}(s)$ can be written as:

$$G_{\Gamma_x x}(s) = \frac{bs}{(1 + \bar{a}K_d)s^2 + (a + \bar{a}K_p)s + \bar{a}K_i}, \tag{6.22}$$

where $\bar{a} = ak_{AOD_x}k_x$. The analysis for motion along the y-axis is identical to that described here.

A number of different methods can be used to tune the PID controller gains to maximize performance based on the transfer function, (6.22) (e.g., see [82]). Here, the control gains are selected based on the H_∞ and H_2 norms for (6.22), which can be written in closed form for this system. The H_∞ norm of $G_{\Gamma_x x}$, $|G_{\Gamma_x x}|_\infty$, represents the maximum amplitude of $|G_{\Gamma_x x}|$, and can be viewed as the largest standard deviation of the particle displacement at any given frequency. The expression can be shown to be:

$$\|G_{\Gamma_x x}\|_\infty = \frac{b}{a + \bar{a}K_p}, \tag{6.23}$$

where the maximum is located at $\omega = \sqrt{\bar{a}K_i/(1 + \bar{a}K_d)}$ (see [49] for details on this derivation of this expression and those that follow). Therefore, the H_∞ norm of the particle motion can only be reduced by increasing K_p, but its location in frequency is determined by both K_i and K_d.

The H_2 norm of $G_{\Gamma_x x}$ is the root mean square, or standard deviation, of the particle displacement. The resulting expression is:

$$\|G_{\Gamma_x x}\|_2 = \frac{b}{\sqrt{2(a + \bar{a}K_p)(1 + \bar{a}K_d)}}. \tag{6.24}$$

It is clear that both K_p and K_d can be used to reduce the standard deviation, while K_i has no effect.

The PID control system was implemented on the trapping instrument described above using an analog PID controller with 100 kHz bandwidth. The x- and y-axes were controlled simultaneously using the same controller gain values. The power spectrum of the motion of the particle in the trap was fit to the reduced-order model (6.11) using least-squares parameter estimation, where the cutoff frequency is $\omega_c = k/\beta$ (see [4]). In this case, $\omega_c = 1{,}046.0\,\text{rad/s}$ for 30 mW laser intensity, so $k = 9.56 \times 10^{-6}\,\text{N/m}$. Using Stokes' law, $\beta = 9.14 \times 10^{-9}\,\text{N s/m}$ where $\eta = 1.0 \times 10^{-3}\,\text{N s/m}^2$ and $r_p = 0.485\,\mu\text{m}$. The gains for the AOD and associated electronics and the back-focal-detection have been measured to be $k_{AOD_x} = 0.1885\,\mu\text{m/V}$ and $k_x = 2.8781\,\text{V}/\mu\text{m}$, respectively.

The amplitude of Brownian motion (as measured by the quadrant photodiode) when using proportional control is shown in Fig. 6.16 for various K_p values. As expected, an increase in K_p decreases the H_∞ and H_2 norms, where the largest
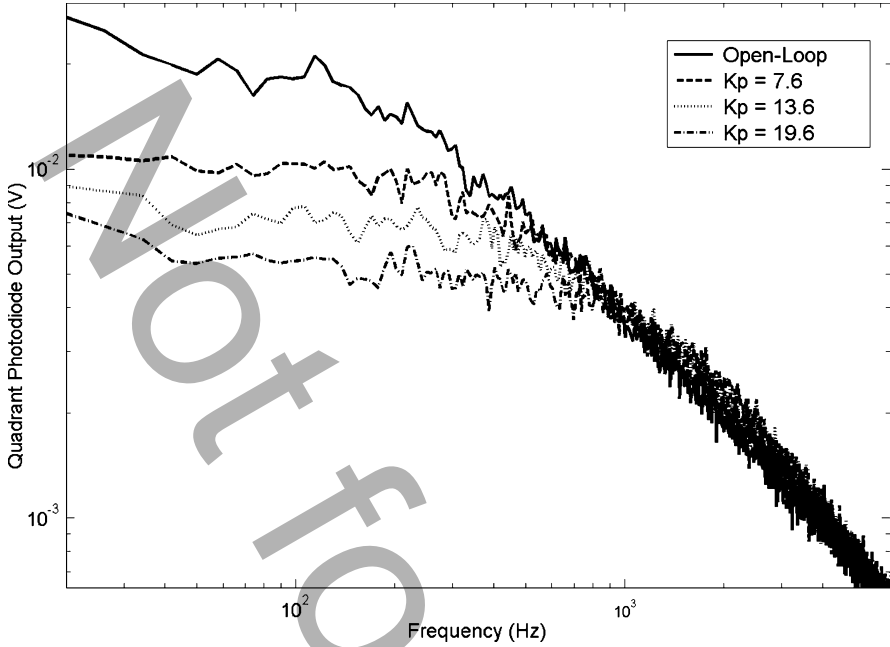
Fig. 6.16 Power spectrum of the Brownian motion of the particle when using proportional control

K_p value reduces the H_∞ norm by 73% and the H_2 norm by 44% compared to the uncontrolled particle (i.e., no feedback).

Results for a proportional–derivative (PD) controller are shown in Fig. 6.17, in comparison with the open-loop case and a proportional controller with the same K_p value ($K_p = 7.6$). Although the PD controller reduces the amplitude out to approximately 2 kHz compared to the proportional controller, the time delay in the acousto-optic deflector electronics causes a spike in the amplitude around 4 kHz. Even so, the PD controller reduces $||G_{\Gamma_x x}||_2$ by 13.1% compared to the proportional controller alone. Finally, results for a proportional–integral (PI) controller are shown in Fig. 6.18 in comparison to the open-loop case and proportional controller with an equivalent K_p value. As predicted by the analysis in the previous section, the integrator has no effect on the H_∞ and H_2 norms. However, the integrator is effective in shifting the particle's energy from one frequency band to another. This would be useful if the particle experiences additional disturbances that were at frequencies below 200 Hz in this example.

Complete PID controllers were also tested but the results did not improve compared to the cases listed here since the PD controller reduces the H_∞ and H_2
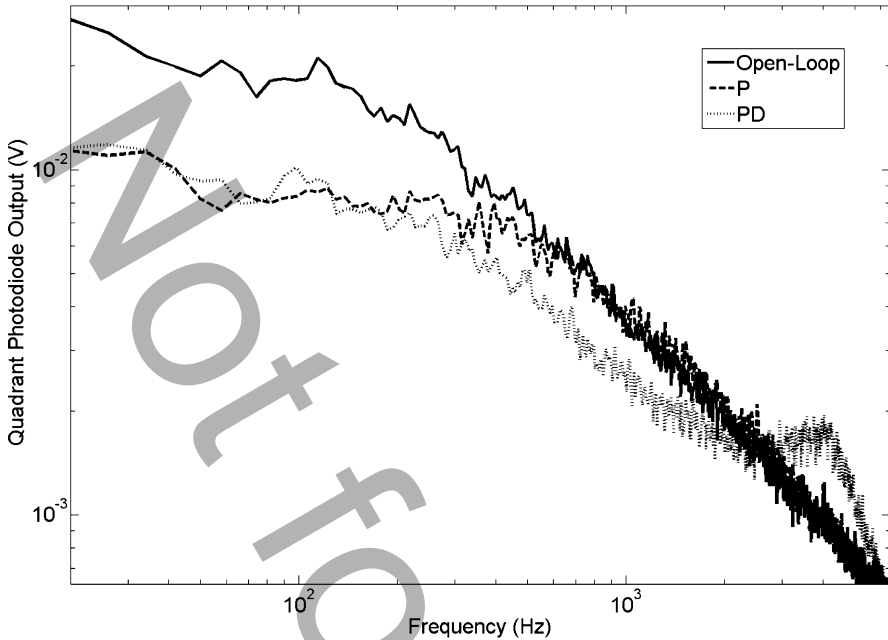
Fig. 6.17 Power spectrum for the Brownian motion of the particle when using a PD controller

norms just as much as the PID controller, as shown in (6.23) and (6.24). However, the addition of the derivative term clearly does provide dissipation of the thermal energy and has a clear benefit over proportional control. Minimizing the time delay in the AODs will increase the effectiveness of the derivative control term. Additional experimental results for the PID controller are presented in [49] and proportional control results are shown in [47].

The PID controller is effective in reducing the Brownian motion of the particle even though the control design was based on a linearized model of the particle dynamics. This is due to the laser intensity used in the experiments, which is moderately high, and the size of the particle, which is approximately $1\,\mu m$ in diameter. Due to these two features, the particle explores a small region in the trap where the dynamics are essentially linear. When the gains are increased, the particle explores a wider region where the forces a more nonlinear and eventually the system becomes unstable due to the use of the approximate model. When using smaller particles and lower laser intensity the particle will be more likely to explore the outer part of the trap and, therefore, the dynamics will be inherently more nonlinear. Under these conditions, it is unclear how effective the PID controller will be in suppressing Brownian motion.
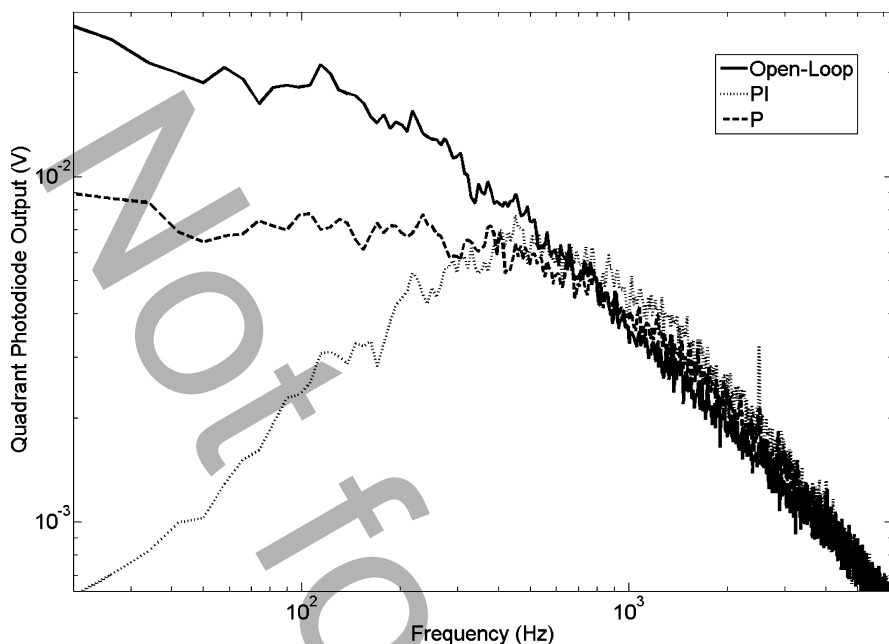
Fig. 6.18 Power spectrum for the Brownian motion of the particle when using a PI controller

6.6 Research Challenges and Future Directions

This chapter has presented an overview of optical trapping and results on the control of optically trapped particles. As with so many servo control problems, feedback control has been shown to provide significant performance benefits in optical trapping and has the potential to enable numerous new capabilities. In many ways, the integration of control systems with optical trapping is in its infancy, with only the most basic analysis and implementations pursued to date. Before closing, we end with a discussion of some exciting technical challenges and opportunities that could have a large impact on the field if solved.

6.6.1 Three-Dimensional Position Control

All of the implementations of feedback control in gradient force optical trapping reported to date have been two dimensional. Achieving three-dimensional position control will open many new applications. However, adding control along the *z*-axis requires a suitable actuator. As described in Sect. 6.3.1, there are only a few scanning actuator options for the *z*-axis and none of them have been demonstrated for high-bandwidth controlled optical trapping. Although intensity control can alter the

trapping dynamics along the *z*-axis, it can only be used to improve the localization of the particle about the center of the trap. It cannot change the vertical position of the trap, which is desirable in manipulation applications. Some combination of both scanning and intensity control that exploits the coupling between these actuation approaches is needed for three-dimensional position control.

6.6.2 Extending Trapping Lifetime

In Sect. 6.4.1, it was shown that a trapped particle will exit the trap in finite time due to Brownian motion and the fact that the trap is a finite-depth potential well. The scanning control approach discussed in Sect. 6.5.1 can reduce the Brownian motion of the particle but it also narrows the effective width of the trap while maintaining the same potential depth. As a result, the particle's time in the trap, or lifetime, is shortened. Nonlinear control methods that can simultaneously reduce particle Brownian motion and increase trapping lifetime must be developed. Intensity control appears to be the best method for increasing trapping lifetime because it can control the potential depth of the trap, which increases the trapping forces along all three axes [53].

6.6.3 Controlled Trapping of Nanoparticles

Almost all of the work on controlled optical trapping has been with particles that are 1 µm in diameter or larger. However, nanoparticle research could strongly benefit from the manipulation capabilities offered by optical trapping. It is known that the trapping lifetime for nanoparticles is fairly short in comparison to the microparticles because the trapping forces decrease strongly with the diameter of the particle. Feedback control could be used to localize nanoparticles if the forces can be modeled and adequate position sensitivity can be achieved with laser-based sensing methods (i.e., the sensitivity also decreases with particle diameter). Reliable nanoparticle trapping could be used to print catalysts for nanowire growth and to observe the absorption of nanoparticles into living cells for toxicological studies, among many other applications.

6.6.4 Trapping in Air and Vacuum

Optical trapping of particles has been almost exclusively pursued in liquids because (1) the biophysical experiments of interest must be performed in liquid, (2) the viscous damping provide by the liquid makes the trap more stable, and (3) the liquid trapping medium facilitates the introduction of particles into the trap.

However, there is interest in trapping in both air and vacuum for nanoassembly applications and for fundamental studies in quantum mechanics [32]. The biggest challenge in trapping in air or vacuum is that the lack of damping, which radically changes the particle dynamics, turning the system into a nonlinear lightly damped oscillator. Depending on the trap strength, the oscillations can be large enough to immediately eject the particle from the trap. Advances in trap modeling, high-bandwidth oscillation control systems, and sample handling must be pursued to make trapping in air and vacuum more reliable.

6.6.5   Nonlinear Stochastic Control Theory

A particle in an optical trap is a nonlinear stochastic system with fairly complex dynamics. Most of the work to date has simplified the problem by either linearizing the system or by excluding the stochastic terms within the stability analysis. A complete stability analysis of the nonlinear stochastic system is needed, in which the stability of the probability distribution of the trapped particle is investigated and the performance of trapping lifetime and position variance is determined as a function of the controller parameters. It is unclear whether the existing control theory can be applied to this problem or whether there is a need for the development of new theory.

The challenges described here are important for optical trapping but also from a general control systems perspective because they are found in many other micro- and nanoscale applications (e.g., nonlinear stochastic control, Brownian motion, and finite escape time). Upon solving them, the resulting innovations must be fed back into the optical trapping applications that have motivated the use of feedback control in the first place. It is expected that the resulting new control approaches will enable exciting new applications of optical trapping in the areas of nanomanufacturing and biophysics, among others.

References

1. A. Ashkin. History of optical trapping and manipulation of small-neutral particle, atoms, and molecules. *IEEE J. Sel. Top. Quantum Electron.*, 6:841–856, 2000.
2. D.C. Grier. A revolution in optical manipulation. *Nature*, 424:810–816, 2003.
3. K.C. Neuman and S.M. Block. Optical trapping. *Rev. Sci. Instrum.*, 75:2787–2809, 2004.
4. K. Visscher, S.P. Gross, and S.M. Block. Construction of multiple-beam optical traps with nanometer-resolution position sensing. *IEEE J. Sel. Top. Quantum Electron.*, 2:1066–1076, 1996.
5. A. Ashkin, J.M. Dziedzic, J.E. Bjorkhom, and S. Chu. Observation of a single-beam gradient force optical trap for dielectric particles. *Opt. Lett.*, 11:288–290, 1986.
6. D.T. Gillespie. The mathematics of Brownian motion and Johnson noise. *Am. J. Phys.*, 64: 225–240, 1995.

 7. R.M. Mazo. *Brownian motion: Fluctuations, dynamics and application*, New York, Oxford, 2002.
 8. A. Ashkin. Forces of a single-beam gradient laser trap on a dielectric sphere in the ray optics regime. *Biophys. J.*, 61:569–582, 1992.
 9. A. Rohrbach. Stiffness of optical traps: Quantitative agreement between experiment and electromagnetic theory. Phys. Rev. Lett., 95:168102, 2005.
10. A.A.R. Neves et al. Electromagnetic forces for an arbitrary optical trapping of a spherical dielectric. *Opt. Express*, 14:13101–13106, 2006.
11. G. Gouesbet, B. Maheu, and G. Grehan. Light-scattering from a sphere arbitrarily located in a Gaussian beam, using a Bromwich formulation. *J. Opt. Soc. Am. A*, 5:1427–1443, 1988.
12. J.A. Lock. Calculation of the radiation trapping force for laser tweezers by use of generalized Lorenz–Mie Theory. I. Localized model description of an on-axis tightly focused laser beam with spherical aberration. *Appl. Opt.*, 43:2532–2544, 2004.
13. K. Svoboda and S.M. Block. Optical trapping of metallic Rayleigh particles. *Opt. Lett.*, 19: 930–932, 1994.
14. Y. Seol, A.E. Carpenter, and T.T. Perkins. Gold nanoparticles: enhanced optical trapping and sensitivity coupled with significant heating. *Opt. Lett.*, 31:2429–2431, 2006.
15. Y. Liu, D.K. Cheng, G.J. Sonek, M.W. Berns, C.F. Chapman, and B.J. Tromberg. Evidence for localized cell heating induced by infrared optical tweezers. *Biophys. J.*, 68:2137–2144, 1995.
16. K.C. Neuman, E.H. Chadd, G.F. Liou, K. Bergman, and S.M. Block. Characterization of photodamage to *Escherichia coli* in optical traps. *Biophys. J.*, 77:2856–2863, 1999.
17. P.M. Hansen, V.K. Bhatia, N. Harrit, and L. Oddershede. Expanding the optical trapping range of gold nanoparticles. *Nano Lett.*, 5:1937–1942, 2005.
18. A. Balijepalli, T.W. LeBrun, and S.K. Gupta. A flexible system framework for a nanoassembly cell using optical tweezers. *Proceedings of the ASME IDETC/CIE*, Philadelphia, PA, 2006, DETC2006–99563.
19. M.D. Wang, H. Yin, R. Landick, J. Gelles, and S.M. Block. Stretching DNA with optical tweezers. *Biophys. J.*, 72:1335–1346, 1997.
20. M.D. Wang, M.J. Schnitzer, H. Yin, R. Landick, J. Gelles, and S.M. Block. Force and velocity measured for single molecules of RNA polymerase. *Science*, 282:902–907, 1998.
21. C. Cecconi, E.A. Shank, C. Bustamante, and S. Marqusee. Direct observation of the three-state folding of a single protein molecule. *Science*, 309:2057–2060, 2005.
22. J.T. Finer, R.M. Simmons, and J.A. Spudich. Single myosin molecule mechanics: piconewton forces and nanometer steps. *Nature*, 368:113–119, 1994.
23. K. Visscher, M.J. Schnitzer, and S.M. Block. Single kinesin molecules studied with a molecular force clamp. *Nature*, 400:184–189, 1999.
24. J. Sleep, D. Wilson, R. Simmons, and W. Gratzer. Elasticity of the red cell membrane and its relation to hemolytic disorders: an optical tweezers study. *Biophys. J.*, 77:3085–3095, 1999.
25. M. Dao, C.T. Lim, and S. Suresh. Mechanics of the human red blood cell deformed by optical tweezers. *J. Mech. Phys. Solids*, 51:2259–2280, 2003.
26. M.M. Wang et al. Microfluidic sorting of mammalian cells by optical force switching. *Nat. Biotechnol.*, 23:83–87, 2005.
27. B.A. Nemet and M. Cronin-Golomb. Microscopic flow measurements with optically trapped probes. *Opt. Lett.*, 27:1357–1359, 2002.
28. B.A. Nemet, Y. Shabtai, and M. Cronin-Golomb. Imaging microscopic viscosity with confocal scanning optical tweezers. *Opt. Lett.*, 27:264–266, 2002.
29. L.P. Ghislain and W.W. Webb. Scanning-force microscope based on an optical trap. *Opt. Lett.*, 18:1678–1680, 1993.
30. M.E.J. Friese, A.G. Truscott, H. Rubinsztein, and N.R. Heckenberg. Three-dimensional imaging with optical tweezers. *Appl. Opt.*, 38:6597–6603, 1999.
31. A. Rohrbach, C. Tischer, D. Neumayer, E.-L. Florin, and E.H.K. Stelzer. Trapping and tracking a local probe with a photonic force microscope. *Rev. Sci. Instrum.*, 75:2197–2210, 2004.
32. T. Li, S. Kheifets, D. Medellin, and M.G. Raizen. Measurement of the instantaneous velocity of a Brownian particle. *Science*, 328:1673–1675, 2010.

33. R.E. Holmlin, M. Schiavoni, C.Y. Chen, S.P. Smith, M.G. Prentiss, and G.M. Whitesides. Light-driven microfabrication: assembly of multicomponent, three-dimensional structures by using optical tweezers. *Angew. Chem. Int. Ed.*, 39:3503–3506, 2000.

34. A. Terray, J. Oakey, and D.W.M. Marr. Fabrication of linear colloidal structures for microfluidic applications. *Appl. Phys. Lett.*, 81:1555–1557, 2002.

35. P.J. Rodrigo, L. Kelemen, C.A. Alonzo, I.R. Perch-Nielsen, J.S. Dam, P. Ormos, and J. Glückstad. 2D optical manipulation and assembly of shape-complementary planar microstructures. *Opt. Express*, 15:9009–9014, 2007.

36. R. Agarwal, K. Ladavac, Y. Roichman, G. Yu, C.M. Lieber, and D.G. Lieber. Manipulation and assembly of nanowires with holographic optical traps. *Opt. Express*, 13:8906–8912, 2005.

37. P.J. Pauzauskie, A. Radenovic, E. Trepagnier, H. Shroff, P. Yang, and J. Liphardt. Optical trapping and integration of semiconductor nanowire assemblies in water. *Nat. Mater.*, 5: 97–101, 2006.

38. M.J. Guffey and N.F. Scherer. All-optical patterning of Au nanoparticles on surfaces using optical traps. *Nano Lett.*, 10:4302–4308, 2010.

39. A. Ashkin and J.M. Dziedzic. Feedback stabilization of optically levitated particles. *Appl. Phys. Lett.*, 30:202–204, 1977.

40. J.E. Molloy, J.E. Burns, J. Kendrick-Jones, R.T. Tregear, and D.C.S. White. Movement and force produced by a single myosin head. *Nature*. 378:209–212, 1995.

41. R.M. Simmons, J.T. Finer, S. Chu, and J.A. Spudich. Quantitative measurements of force and displacement using an optical trap. *Biophys. J.*, 70:1813–1822, 1996.

42. W.H. Guilford, D.E. Dupuis, G. Kennedy, J. Wu, J.B. Patlak, and D.M. Warshaw. Smooth muscle and skeletal muscle myosins produce similar unitary forces and displacements in the laser trap. *Biophys. J.*, 72:1006–1021, 1997.

43. K. Visscher and S.M. Block. Versatile optical traps with feedback control. *Methods Enzymol.*, 298:460–489, 1998.

44. M.J. Lang, C.L. Asbury, J.W. Shaevitz, and S.M. Block. An automated two-dimensional optical force clamp for single molecule studies. *Biophys. J.*, 83:491–501, 2002.

45. K.D. Wulff, D.G. Cole, and R.L. Clark. Servo control of an optical trap. *Appl. Opt.*, 46: 4923–4931, 2007.

46. K.D. Wulff, D.G. Cole, and R.L. Clark. Adaptive disturbance rejection in an optical trap. *Appl. Opt.*, 47:3585–3589, 2008.

47. A.E. Wallin, H. Ojala, E. Hæggström, and R. Tuma. Stiffer optical tweezers through real-time feedback control. *Appl. Phys. Lett.*, 92:224104, 2008.

48. H. Ojala, A. Korsbäck, A.E. Wallin, and E. Hæggström. Optical position clamping with predictive control. *Appl. Phys. Lett.*, 95:181104, 2009.

49. J.J. Gorman, A. Balijepalli, and T.W. LeBrun. Control of optically trapped particles for Brownian motion suppression. *IEEE Trans. Control Syst. Technol., in press*, 2011.

50. A. Ranaweera, B. Bamieh, and A.R. Teel. Nonlinear stabilization of a spherical particle trapped in an optical tweezer. *IEEE Conference on Decision and Control*, Maui, HI, 2003, 3431–3436.

51. A. Ranaweera and B. Bamieh. Modeling, identification, and control of a spherical particle trapped in an optical tweezer. *Int. J. Robust Nonlinear Control*, 15:747–768, 2005.

52. C. Aguilar-Ibañez, M.S. Suarez-Castanon, and L.I. Rosas-Soriano. A simple control scheme for the manipulation of a particle by means of optical tweezers. *Int. J. Robust Nonlinear Control*, 21:328–337, 2011.

53. A.K. Balijepalli. *Modeling and experimental techniques to demonstrate nanomanipulation with optical tweezers*. Ph.D. Thesis, University of Maryland, 2011.

54. E Fallman and O Axner. Design for fully steerable dual-trap optical tweezers. *Appl. Opt.*, 36:2107–2113, 1997.

55. E.R. Dufresne, G.C. Spalding, M.T. Dearing, S.A. Sheets, and D.G. Grier. Computer-generated holographic optical tweezer arrays. *Rev. Sci. Instrum.*, 72:1810–1816, 2001.

56. P.J. Rodrigo, V.R. Daria, and J. Glückstad. Real-time three-dimensional optical micromanipulation of multiple particles and living cells. *Opt. Lett.*, 29:2270–2272, 2004.

57. A.P. Goutzoulis and D.R. Pape. *Design and fabrication of acousto-optic devices*, New York, Marcel Dekker, 1994.
58. M. Gottlieb, C.L.M. Ireland, and J.M. Ley. *Electro-optic and acousto-optic scanning and deflection*, New York, Marcel Dekker, 1983.
59. M.T. Valentine, N.R. Guydosh, B. Gutiérrez-Medina, A.N. Fehr, J.O. Andreasson, and S.M. Block. Precision steering of an optical trap by electro-optic deflection. *Opt. Lett.*, 33:599–601, 2008.
60. N. Kaplan, A. Friedman, and N. Davidson. Acousto-optic lens with very fast focus scanning. *Opt. Lett.*, 26:1078–1080, 2001.
61. V.X.D. Yang et al. Doppler optical coherence tomography with a micro-electro-mechanical membrane mirror for high-speed dynamic focus tracking. *Opt. Lett.*, 31:1262–1264, 2006.
62. F. Gittes and C.F. Schmidt. Interference model for back-focal-plane displacement detection in optical tweezers. *Opt. Lett.*, 23:7–9, 1998.
63. M.W. Allersma, F. Gittes, M.J. deCastro, R.J. Stewart, and C.F. Schmidt. Two-dimensional tracking for ncd motility by back focal plane interferometry. *Biophys. J.*, 74:1074–1085, 1998.
64. L. Nugent-Glandorf and T.T. Perkins. Measuring 0.1 nm motion in 1 ms in an optical microscope with differential back-focal-plane detection. *Opt. Lett.*, 29:2611–2613, 2004.
65. W. Denk and W.W. Webb. Optical measurement of picometer displacements of transparent microscopic objects. *Appl. Opt.*, 29:2382–2391, 1990.
66. K. Svoboda, C.F. Schmidt, B.J. Schnapp, and S.M. Block. Direct observation of kinesin stepping by optical trapping interferometry. *Nature*, 365:721–727, 1993.
67. J.C. Crocker and D.G. Grier. Methods of digital video microscopy for colloidal studies. *J. Colloid Interface Sci.*, 179:298–310, 1996.
68. M.K. Cheezum, W.F. Walker, and W.H. Guilford. Quantitative comparison of algorithms for tracking single fluorescent particles. *Biophys. J.*, 81:2378–2388, 2001.
69. M. Capitanio, R. Cicchi, and F.S. Pavone. Position control and optical manipulation for nanotechnology applications. *Eur. Phys. J. B*, 46:1–8, 2005.
70. O. Otto, C. Gutsche, F. Kremer, and U.F. Keyser. Optical tweezers with 2.5 kHz bandwidth video detection for single-colloid electrophoresis. *Rev. Sci. Instrum.*, 79:023710, 2008.
71. L.P. Ghislain, N.A. Switz, and W.W. Webb. Measurement of small forces using an optical trap. *Rev. Sci. Instrum.*, 65:2762–2768, 1994.
72. I.M. Peters, B.G. de Grooth, J.M. Schins, C.G. Figdor, and J. Greve. Three dimensional single-particle tracking with nanometer resolution. *Rev. Sci. Instrum.*, 69:2762–2766, 1998.
73. A. Pralle, M. Prummer, E.-L. Florin, E.H.K. Stelzer, and J.K.H. Hörber. Three-dimensional high-resolution particle tracking for optical tweezers by forward scattered light. *Microsc. Res. Tech.*, 44:378–386, 1999.
74. A. Rohrbach and E.H.K. Stelzer. Three-dimensional position detection of optically trapped dielectric particles. *J. Appl. Phys.*, 91:5474–5488, 2002.
75. F. Gittes and C.F. Schmidt. Signals and noise in micromechanical measurements. *Methods in Cell Biol.*, 55:129–156, 1998.
76. A. Rohrbach and E.H.K. Stelzer. Trapping forces, force constants, and potential depths for dielectric spheres in the presence of spherical aberrations. *Appl. Opt.*, 41:2494–2507, 2002.
77. H. Risken. *The fokker-planck equation: Methods of solution and applications*. New York, Springer, 1996.
78. Y.K. Nahmias and D.J. Odde. Analysis of radiation forces in laser trapping and laser-guided direct writing applications. *IEEE J. Quantum Electron.*, 38:131–141, 2002.
79. A. Balijepalli, T.W. Lebrun, and S.K. Gupta. Stochastic simulations with graphics hardware: Characterization of accuracy and performance. *J. Comput. Inf. Sci. Eng.*, 10: 011010, 2010.
80. J.H. Ginsberg, *Advanced engineering dynamics*, 2nd edition, New York, NY, Cambridge University Press, 1995.
81. B.J. Kuo, *Automatic Control Systems*, 7th edition, Englewood Cliffs, NJ, Prentice-Hall, 1995.
82. K.J. Åström and T. Hägglund, *Advanced PID control*, Research Triangle Park, NC, ISA, 2005.